

Parameterizing Unresolved Mesoscale Motions in Atmospheric Dispersion Models

HELEN N. WEBSTER, THOMAS WHITEHEAD,^a AND DAVID J. THOMSON

Met Office, Exeter, United Kingdom

(Manuscript received 22 March 2017, in final form 8 December 2017)

ABSTRACT

In atmospheric dispersion models driven by meteorological data from numerical weather prediction (NWP) models, it is necessary to include a parameterization for plume spread that is due to unresolved mesoscale motions. These are motions that are not resolved by the input NWP data but are larger in size than the three-dimensional turbulent motions represented by turbulence parameterizations. Neglecting the effect of these quasi-two-dimensional unresolved mesoscale motions has been shown to lead to underprediction of plume spread and overprediction of concentrations within the plume. NWP modeling is conducted at a range of resolutions that resolve different scales of motion. This suggests that any parameterization of unresolved mesoscale motions should depend on the resolution of the input NWP data. Spectral analysis of NWP data and wind observations is used to assess the mesoscale motions unresolved by the NWP model. Appropriate velocity variances and Lagrangian time scales for these motions are found by calculating the missing variance in the energy spectra and analyzing correlation functions. A strong dependence on the resolution of the NWP data is seen, resulting in larger velocity variances and Lagrangian time scales from the lower-resolution models. A parameterization of unresolved mesoscale motions on the basis of the NWP resolution is proposed.

1. Introduction

Variations in wind direction caused by quasi-two-dimensional horizontal eddies can play an important role in plume dispersion. These mesoscale eddies are not suppressed by stability forces and are often attributed to gravity waves, terrain interactions with the flow, mesoscale rolls and cell patterns in the synoptic flow, or surface inhomogeneities (Hanna 1983). They are particularly important in stable light wind conditions when they dominate the transport and dispersion of a plume, but they make some contribution under all atmospheric conditions. In this paper we discuss the effect of atmospheric motions of these scales on plume dispersion and methods for parameterizing these effects in atmospheric dispersion models. Spectral analysis techniques are used to infer appropriate parameterizations for dispersion models using input numerical weather prediction (NWP) meteorological data of differing resolutions. Higher-resolution NWP models are able to resolve

smaller-scale atmospheric motions, and a parameterization should only represent the effect of those motions that are missing from the input meteorological data. The range of motions considered here is resolved to varying degrees by NWP models, and hence there is an expectation that the parameterization of unresolved mesoscale motions will be dependent on the NWP model resolution. An early version of this work appears as a Met Office technical report (Webster et al. 2015) and includes further discussion and details of the results presented here. This technical report constitutes part of the documentation for the Met Office's atmospheric dispersion model, Numerical Atmospheric-Dispersion Modelling Environment (NAME), and, as such, it has a particular focus providing specific and detailed model information. While in progress, this work was presented at conferences (Webster and Thomson 2005; Webster et al. 2014). Here we present this work in a general modeling context, although there is a degree of overlap with the technical report and the conference abstracts.

2. Plume meandering

The effect of mesoscale atmospheric motions on plumes is usually to cause, at least relatively close to the source, a slow meandering of the plume, in which the instantaneous plume may be thin but over a time period of

^a Current affiliation: Theory of Condensed Matter Group, Department of Physics, Cavendish Laboratory, University of Cambridge, Cambridge, United Kingdom.

Corresponding author: Helen N. Webster, helen.webster@metoffice.gov.uk

an hour or more may meander over a wide angle. Plume meandering moves the plume around as a whole and does not disperse the plume or affect its internal structure. Observed concentrations in regions of meandering plumes are often characterized by periods of zero concentrations interspersed by periods of relatively high concentrations (Mylne and Mason 1991; Mylne 1992). Hourly averaged plumes are considerably wider and have lower concentrations than observed within the instantaneous plume. The mesoscale motions that cause plume meandering near to the source can, however, result in plume diffusion farther downwind when the width of the plume has, because of diffusion by small-scale turbulent eddies, increased to be comparable in size to the mesoscale eddies.

These two-dimensional mesoscale motions are particularly relevant in stable light wind conditions when they are the dominant cause of lateral spread of a plume. However, the motions are usually neither resolved by the meteorological data used to drive atmospheric dispersion models nor covered by parameterizations of small-scale three-dimensional turbulent motions. It has been shown that neglecting these intermediate-scale motions leads to an underestimation of plume spread (Gupta et al. 1997) and an overestimation of air concentrations (Maryon 1997). Indeed, Kristensen et al. (1981) suggest that, in strongly stable conditions with low wind speeds, estimates of mean concentrations can easily be a factor of 4–6 too high if these motions are not taken into account. It is important, therefore, to parameterize these unresolved mesoscale motions within atmospheric dispersion models.

A number of experiments have been conducted to study wind direction variability over different time periods and at a range of locations with varying terrain. Large variations in wind direction have been observed in stable light wind conditions (Smith and Abbott 1961; Schacher et al. 1982; Moore 1975, 1976; Hanna 1983, 1990; Davies and Thomson 1999). At Porton, United Kingdom, Smith and Abbott (1961) observed that the wind direction variability increased at night as winds became light. The standard deviation of the lateral wind velocity (σ_v) was relatively insensitive to both wind speed and stability and was found to have a constant value of 0.3 m s^{-1} for all wind speeds in stable conditions. At a complex terrain site in California, Hanna (1981a) found similarly that a constant value for σ_v , independent of wind speed, was appropriate during nighttime conditions. However, a larger value for σ_v than was obtained at Porton by Smith and Abbott (1961) was found at this site ($\sigma_v \sim 1 \text{ m s}^{-1}$) and attributed to lateral eddies induced by the terrain. For an overwater diffusion experiment performed off the Californian coast, Schacher et al. (1982) found that the wind

direction variability was large and variable during stable conditions. Here a representative σ_v value of about 0.5 m s^{-1} was found by Hanna (1983) to be appropriate. Overnight experiments on a flat plain in the Snake River basin in Idaho suggested hourly averaged σ_v values of $\sim 0.5 \text{ m s}^{-1}$ (Hanna 1983). Hanna (1983, 1990) provides evidence that his formula for wind direction variability over time periods of 1 h, namely,

$$\frac{\sigma_v}{u} = \tan(\sigma_\theta) = \frac{0.5 \text{ m s}^{-1}}{u},$$

is valid over all types of terrain with the large values of wind direction variability (σ_θ) over complex terrain being due to lower wind speeds u . He notes, however, that, for individual sites, σ_v values typically exhibit a scatter of about $\pm 0.3 \text{ m s}^{-1}$ about the $\sigma_v \sim 0.5 \text{ m s}^{-1}$ relationship. Over longer time periods of several hours, larger-scale meso- and synoptic-scale eddies contribute to variation in the wind direction. Based on dispersion experiments in the United Kingdom, Moore (1975, 1976) proposed parameterizations of wind variability over a range of time periods up to 24 h,

$$\sigma_\theta = 0.065 \left(\frac{7}{u_{10m}} T_A \right)^{1/2}, \quad (1)$$

where T_A is the averaging time in hours and u_{10m} is the magnitude of the average 10-m wind velocity over the same period.

Measurements of wind direction variability from these experiments and the reported formulas have been used as the basis for parameterizations of two-dimensional mesoscale motions within atmospheric dispersion models. Moore's parameterization [Eq. (1)] has been widely used in dispersion modeling in the United Kingdom [e.g., in the short-range models "R91" (Clarke 1979) and Atmospheric Dispersion Modelling System (ADMS; Carruthers et al. 1994)]. For many years, $\sigma_v = 0.5 \text{ m s}^{-1}$ (as suggested by Hanna 1983, 1990) was used in the Lagrangian dispersion model NAME (Jones et al. 2007). The Lagrangian dispersion model known as "FLEXPART" (Stohl 2000; Stohl et al. 2005) analyses the variability in the input grid-scale winds surrounding the particle location to estimate a suitable value for σ_v .

3. Parameterizations in atmospheric dispersion models

The aim of including a parameterization of unresolved mesoscale motions in atmospheric dispersion models is to represent diffusion by motions in the intermediate

frequency range between the motions resolved by the input meteorological data and small-scale three-dimensional turbulent eddies. In reality, however, turbulent diffusion cannot be split into well-defined spatial scales corresponding to diffusion by resolved motions, unresolved mesoscale motions, and turbulent fluctuations. The input meteorological data for atmospheric dispersion models commonly comes from NWP models of differing resolutions. According to Maryon (1998), the required parameterization for unresolved mesoscale motions is mainly constrained by the time resolution of the input wind fields,¹ which tends to be coarse in comparison with their spatial resolution. For input wind fields with a time resolution of ΔT_f , the highest-frequency motions that can be resolved are those of period $2\Delta T_f$ (although this is complicated by the fact that, for low-frequency but instantaneous data from the NWP model, the higher frequencies resolved by the NWP model will be aliased to lower frequencies rather than discarded). Furthermore, it is often not explicitly stated in the literature for which scales the turbulence parameterizations have been developed (Stohl 2000). The result is an intermediate frequency range between the resolved and turbulent motions that is not well defined and is dependent on the input meteorological data and perhaps even the turbulence parameterization chosen.

Dispersion due to unresolved mesoscale processes can be represented in most types of dispersion model, given information on the velocity variance of the unresolved motions and their correlation time scale. For example, in Eulerian models one can use these quantities to estimate the (horizontal) diffusivity due to unresolved mesoscale motions, which can be added to any other diffusivity in the model. In Lagrangian models such as NAME (Jones et al. 2007) an extra stochastic component can be added to the motion of the Lagrangian particles, independent from any stochastic component used to represent the turbulence. For example, at short ranges NAME uses an extra fluctuating horizontal velocity \mathbf{u}_m with independent components, each having an appropriate standard deviation σ_u and integral time scale τ_u and evolving according to a Langevin equation

$$du_{m,i} = -\left(\frac{u_{m,i}}{\tau_u}\right)dt + \sqrt{\frac{2\sigma_u^2}{\tau_u}}dW_i,$$

where the dW_i are the increments of independent Wiener processes with mean zero and variance dt and $i = 1$

and 2 indicate the two horizontal components. This is then added to the other elements of the particle's velocity (primarily mean advection and turbulence). At long range, a diffusive process is used with increments $d\mathbf{x}_m$ in the particle's horizontal position corresponding to a diffusivity K_u , that is,

$$dx_{m,i} = \sqrt{2K_u}dW_i, \quad i = 1, 2.$$

At large travel times t , $K_u = \sigma_u^2\tau_u$. However, we damp the diffusivity near to the source with $K_u = \sigma_u^2\tau_u[1 - \exp(-t/\tau_u)]$ to improve the prediction when $t \lesssim \tau_u$. The u and v components ($i = 1$ and 2) of the velocity variance, Lagrangian time scale, and diffusivity are taken to be equivalent. For both long and short range, the mean wind is obtained from the input NWP meteorological data and is interpolated in both time and space to the particle position at each time step. The dispersion model time step typically takes values between 1 and 15 min, although shorter time steps can be enforced for more accurate modeling at short range. Finally, a terrain-following coordinate system is used, with the velocity \mathbf{u}_m and position increment $d\mathbf{x}_m$ acting to change the horizontal position but not the terrain-following vertical coordinate.

Our aim in this paper is to estimate appropriate σ_u , τ_u , and K_u values for unresolved mesoscale motions from wind velocity time series obtained from observations and from NWP simulations, which will be suitable for use in parameterizations within atmospheric dispersion models. In principle the diffusivity and standard deviation could be made tensor quantities, potentially with off-diagonal components, but we do not investigate such directional dependences here. We use spectra and correlation functions to study the motions resolved by the NWP data, in order to gain some understanding of the missing motions that need to be parameterized. Both boundary layer and free-troposphere data are considered. NWP data from different NWP models (Met Office and ECMWF; global and limited area) and with various spatial and temporal resolutions are analyzed for a range of years.

4. Boundary layer motions

Hourly “spot” (in reality, 10-min mean) wind observations at a height of 10 m above ground level (AGL) at Heathrow (51.48°N, 0.45°W), Wattisham (52.12°N, 0.96°E), and Aviemore (57.21°N, 3.83°W) in the United Kingdom have been obtained from the Met Office's observations archive for a selection of years between 1998 and 2012. In general, missing values account for a

¹ The time interval between consecutive wind fields in the data feed is expected to be much larger than the internal time step of the NWP model.

small proportion of the observations (<2% in most cases), although linear interpolation in time is employed to replace missing data values from any of the sites. Wind observations from the Met Office's Meteorological Research Unit (MRU) at Cardington (52.10°N, 0.42°W), England, were also obtained. The surface site instrumentation at Cardington logged data at a frequency of 4 Hz in 1998–2004 and at a frequency of 10 Hz since 2005, and from a range of observing heights. Data from 10 m AGL are used here. These data are averaged over various (sub-hourly) time intervals and use is made here of data with averaging periods between 10 and 30 min since this enables the atmospheric spectra to be analyzed within the frequency range of mesoscale motions. NWP data were also retrieved at the locations and heights of the observations and, if necessary, linearly interpolated, in the same way as generally done within atmospheric dispersion models, to match the time resolution of the observations.

Energy spectra are generated from yearly time series of the wind components (u and v) for both NWP and observed data. To calculate spectra, a fast Fourier transform routine was used and the variance at frequencies $f = q/(N\Delta t)$, $q = 1, \dots, N/2$ computed, where N is the number of data points in the time series and Δt is the time interval between successive data values. The highest frequency represented (the Nyquist frequency) is $f = 1/(2\Delta t)$. These values were then multiplied by $N\Delta t$ to get the variance spectral density $\phi[f = q/(N\Delta t)]$, which is defined so that the area under the variance spectral density curve (for $f > 0$);

$$\int_0^{\infty} \phi(f) df \approx \sum_{f=1/(N\Delta t)}^{1/(2\Delta t)} \phi(f) \Delta f = \sum_{q=1}^{N/2} \phi\left(\frac{q}{N\Delta t}\right) \frac{1}{N\Delta t}$$

is the total variance. The raw spectral curve is noisy and hence a block averaging method is applied, in which the number of data values to be averaged increases by approximately a factor of 4/3 from one block to the next (i.e., the frequency boundaries of the blocks increase by roughly a factor of 4/3 between blocks). The factor of 4/3 is chosen to be large enough to smooth out the noise but small enough to keep the shape of the spectral curve. We also take the average of the u and v spectra, since we do not distinguish here between the u and v components.

The spectra obtained from NWP data were compared with the spectra obtained from observational data. In comparing the spectra, the NWP spectra are scaled to visually match the observed spectra at low frequencies. This accounts for the fact that local observing site characteristics (e.g., roughness length) may differ from that assumed in the NWP model, and for any anemometer calibration inaccuracies. Figure 1 shows

example plots of NWP and observed horizontal wind spectra for Wattisham and Cardington obtained using data from 2012. NWP data for 2012 are obtained from various configurations of the Met Office's Unified Model (MetUM) including the global model and a range of higher-resolution limited area models (see Table 1). In 2012 the global MetUM had a spatial resolution of $0.3516^\circ \times 0.2344^\circ$ (approximately 25 km in midlatitudes) and the time resolution of the data feed was 3 h. Three limited area models [the North Atlantic and European (NAE), the "4km," and the "UKV"] were available, with the data feed providing hourly input wind fields. The NAE, 4km, and UKV models have spatial resolutions of approximately 12, 4, and 1.5 km, respectively. The higher temporal resolution (10 min) of the (time averaged) observations at Cardington allows the spectra in Fig. 1 to be calculated out to higher frequencies. We also note that, for the hourly "spot" observations at Wattisham, aliasing of high-frequency fluctuations occurs, resulting in the representation of these eddies as lower-frequency motions in the spectral curve. As expected, the spectra generated from NWP data contain less energy at high frequencies than the spectra generated from observational data. The resolution of the NWP model has a noticeable impact on the motions captured at the higher-frequency end, with less variance here in the spectral curve for the lower-resolution models. The spatial resolution of the NWP model and the temporal resolution of the data from the model are both important. There is, however, very little difference between the 4km and UKV model spectra, suggesting that the time resolution of the NWP data fields (both hourly) may be the limiting factor for these models. The variation in the missing variance between the different NWP models is in line with the idea that the parameterization of unresolved mesoscale motions will depend on the NWP model used.

a. Calculating velocity variances

To calculate the missing variance, the area between the two spectral curves is determined over a frequency range from a lower to an upper value. The lower point of the frequency range is given by the point of divergence of the NWP spectra from the observed spectra (illustrated by the colored dashed and dotted vertical lines in Fig. 1). This was determined as the lowest frequency at which the curves differed by 30% of the observed spectra, with some judgment used to exclude occasional high differences at isolated frequencies that are probably due to noise. In addition the point of divergence was restricted to frequencies higher than that corresponding to the diurnal cycle. The upper point of the frequency range could be taken to be the high-frequency end

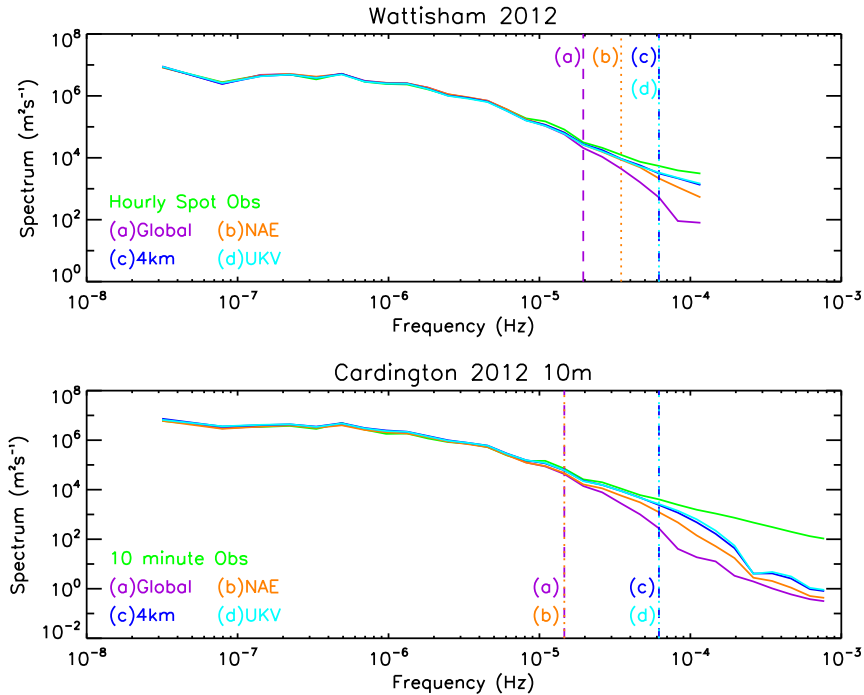


FIG. 1. Example horizontal spectra at heights of 10 m AGL generated from 2012 observations at Wattisham and Cardington and MetUM data [global (25 km, 3 h), NAE (12 km, 1 h), 4km (4 km, 1 h), and UKV (1.5 km, 1 h)]. The dashed and dotted vertical lines [labeled (a)–(d)] indicate the frequency at which the NWP spectra diverge from the observational spectra.

(Nyquist frequency) of the spectral curves or the frequency that the turbulence parameterizations cover, if that was deemed to be lower. Here we choose the upper-frequency point to be the Nyquist frequency of the spectral curves and hence it is dependent on the time resolution of the observations. The highest-frequency observations used here are 10-min averaged winds observed at Cardington with a Nyquist frequency of 8.3×10^{-4} Hz (corresponding to motions with periods of 20 min). Motions of such frequencies may possibly overlap with the frequencies covered by the turbulence parameterizations, particularly in convective conditions.

The lowest-frequency observations used here are hourly “spot” values with a Nyquist frequency of 1.4×10^{-4} Hz (motions with periods of 2 h). However, the hourly “spot” winds are in fact 10-min averages obtained at hourly intervals and hence the variance in the hourly observations will be similar to the variance in observations with a 10-min frequency, with the highest frequencies being represented as lower-frequency motions in the spectral curve because of aliasing. Hence, some sub-two-hourly atmospheric motions, which, on first glance, might be thought to be excluded from the missing variance calculation, are included except for the part

TABLE 1. NWP data used in this study.

Model	Years	Spatial resolution (km)	Temporal resolution (h)
ECMWF ERA-Interim	2008, 2006, 2004, 2001, 2000, 1998	80	3
MetUM global	2004, 2001, 2000	60	3
MetUM regional	1998	50	3
MetUM global	2008, 2006	40	3
MetUM global	2012	25	3
MetUM mesoscale	2000	12	3
MetUM mesoscale	2006, 2004, 2001	12	1
MetUM NAE	2012, 2008	12	1
MetUM 4km	2012, 2008	4	1
MetUM UKV	2012	1.5	1

aliased to below the divergence point. Hence the question of whether the observations include a contribution from turbulent motions applies here too. Fortunately, however, the area between the observed and NWP spectral curves is not strongly influenced by the upper-frequency point (note the use of a log scale on the spectral plots).

b. Calculating Lagrangian time scales

Treating the data as periodic with period $N\Delta t$, the velocity correlation function at time lag $t = m\Delta t$ can be written as

$$R(t) = \sum_{q=1}^{N/2} \phi\left(\frac{q}{N\Delta t}\right) \frac{1}{N\Delta t} \cos\left(\frac{2\pi qt}{N\Delta t}\right) \approx \int_0^{\infty} \phi(f) \cos(2\pi ft) df. \quad (2)$$

We can use this to calculate correlation functions from spectra. To estimate the correlation function of the unresolved motions we calculate the spectra of the observed and NWP time series. The spectra are filtered to remove the low-frequency motions by setting $\phi[q/(N\Delta t)]$ to zero for wavenumbers $q = 0, \dots, (D - 1)$, where $f = D/(N\Delta t)$ is the frequency at which the modeled spectrum is deemed to diverge from the observed spectrum. The difference between the filtered spectra obtained from observations and from NWP model data is calculated, and Eq. (2) is applied to this difference to give the correlation function for the unresolved motions.

The integral of the correlation function cannot be used directly to compute an integral time scale since the correlation function with these periodicity assumptions has zero integral. Hence we need to consider other methods of estimating the integral time scale. We determine the integral time scale from the time at which the correlation function $R(t)$ falls to e^{-1} of its original value $R(0)$ as is appropriate when the correlation function takes the commonly assumed form

$$R(t) = \sigma_u^2 \exp\left(-\frac{t}{\tau_u}\right). \quad (3)$$

The unresolved velocity variances (σ_u^2) can also be determined from this method and are given by the initial value of the correlation function $R(0)$.

Figure 2 shows example correlation functions (normalized by the variance) for the motions corresponding to the missing energy in the 2012 NWP spectra in Fig. 1. These correlation functions show evidence of negative lobes, in line with the oscillatory behavior seen in correlation functions obtained from observational data in other studies (Oettl et al. 2001; Anfossi et al. 2005;

Luhar 2012). It seems likely that this oscillatory behavior is due, at least partly, to the sharp spectral cutoff that is not vastly different to the scales of motion of interest. With a sharp cutoff, the correlation function will have a zero integral scale and so will always have negative lobes, if only a result of the filtering process. Despite this oscillatory behavior, the e -folding time seems an adequate measure of the time scale of the correlation decay for the purpose of estimating the enhanced dispersion.

In general, the higher-resolution NWP models have the smallest predicted time scales for the missing energy, in agreement with the higher frequencies for the point of divergence. The time scale determined by this correlation method, using wind data at a fixed point in space, is an Eulerian time scale (τ_E); the Lagrangian time scale (τ_L) is generally larger than the Eulerian time scale. Pasquill and Smith (1983) and Hanna (1981b) discuss the relationship between Eulerian and Lagrangian time scales. Theory suggests that $\tau_L/\tau_E \propto u/\sigma_u$, and hence smaller values of τ_L/τ_E might be expected in stable, light wind conditions. However, for simplicity (and because our approach only gives a single value of τ_E rather than one that can vary with wind speed and stability) we choose to use $\tau_L/\tau_E = \beta$, where β is a constant value. There is some scatter in β obtained from observations (see Hanna 1981b and references therein). Here we use $\beta = 3$ to determine a Lagrangian time scale from the calculated Eulerian time scale. This value is a midvalue within the range of average values indicated in Hanna (1981b). However, we note that there is some uncertainty in this β value.

c. Boundary layer results

The velocity variances σ_u^2 and Lagrangian time scales τ_u of the unresolved mesoscale motions are obtained using observations at a number of locations and over a number of years and using NWP data from a range of models of differing resolutions (see Table 1). Appropriate diffusivities K_u are determined from the velocity variances and the Lagrangian time scales using $K_u = \sigma_u^2 \tau_u = 3\sigma_u^2 \tau_E$. For some NWP model resolutions, a wide range of values are obtained for the parameters of the missing motions over the sites, years and, for Cardington, averaging times considered here (see Table 2). Smaller velocity variances, Lagrangian time scales and diffusivities are, however, obtained with higher-resolution NWP data. Results obtained from the MetUM and from ERA-Interim at similar resolution are consistent. We recommend the values given in Table 3, which are based on the mean values calculated over the different years, different sites, averaging times, and different NWP models with similar resolution (where appropriate), although there is obviously some

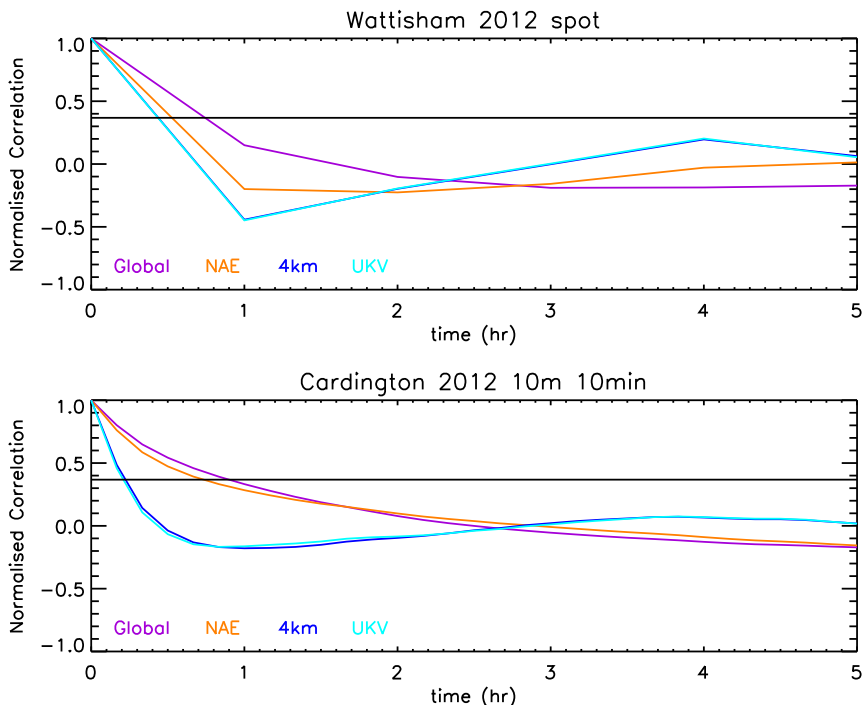


FIG. 2. Example normalized correlation functions for the unresolved mesoscale motions at a height of 10 m AGL at Wattisham and Cardington, generated from 2012 observations and MetUM data [global (25 km, 3 h), NAE (12 km, 1 h), 4km (4 km, 1 h), and UKV (1.5 km, 1 h)]. The horizontal 1/e line (black) is used to determine the time scale.

uncertainty in these parameters because of the range of values obtained.

5. Free-tropospheric motions

Most parameterizations of mesoscale motions are based on near-surface observations and the applicability of these parameterizations within the free troposphere is questionable. In comparison with the boundary layer, mesoscale motions in the free troposphere are not frequently measured. It is a nontrivial exercise to obtain good, reliable, and frequent wind observations over a significant period of time in the free troposphere that are suitable for spectral analysis. Instrumentation on tall towers (such as the 200-m Cabauw tower in the Netherlands) is not situated high enough to consistently

measure above the boundary layer. Radiosondes provide atmospheric profile data but only infrequently (often twice a day) and furthermore, they are advected downwind, and hence do not give observations at a fixed location. Free-tropospheric wind data [atmospheric motion vectors (AMVs)] can be derived from satellite data by tracking tracers (usually clouds or water vapor) through a sequence of images. While this can result in some cases in hourly data, the location and height of observations is variable and determined by the cloud location and cloud top. Furthermore, the resolution is relatively coarse with significant spatial and temporal averaging. In addition, the data can have rather complicated error characteristics. This suggests that satellite-derived wind data are not well suited to the spectral analysis conducted here. Wind data determined

TABLE 2. The ranges of velocity variances ($m^2 s^{-2}$) and diffusivities ($m^2 s^{-1}$) obtained using boundary layer observations.

Models	Resolution	σ_u^2 ($m^2 s^{-2}$)	K_u ($m^2 s^{-1}$)
MetUM global, MetUM regional, and ERA-Interim	≥ 60 km, 3 h	0.63–1.23	5882–16 882
MetUM global	~ 40 km, 3 h	0.66–0.92	5977–9965
MetUM global	~ 20 km, 3 h	0.55–0.81	4905–7911
MetUM mesoscale	~ 10 km, 3 h	0.59–0.98	5350–9466
MetUM mesoscale and MetUM NAE	~ 10 km, 1 h	0.19–0.88	852–10 439
MetUM 4km and MetUM UKV	≤ 4 km, 1 h	0.11–0.42	312–3873

TABLE 3. Recommended parameter values for the parameterization of unresolved mesoscale motions based on NWP model resolution.

Resolution	σ_u^2 ($\text{m}^2 \text{s}^{-2}$)	τ_u (s)	K_u ($\text{m}^2 \text{s}^{-1}$)
≥ 60 km, 3 h	0.90	10 000	9000
~ 40 km, 3 h	0.81	10 000	8100
~ 20 km, 3 h	0.64	10 000	6400
~ 10 km, 3 h	0.64	10 000	6400
~ 10 km, 1 h	0.49	8000	3920
≤ 4 km, 1 h	0.30	6500	1950

from wind profilers, however, result in high-temporal-resolution data at fixed locations, measured at fixed heights, and therefore can be used for spectral analysis. We discuss this data source further in the next section.

a. Wind profiler data

A number of authors have studied the accuracy of horizontal winds measured by wind profilers. These wind observations have been compared with independent measurements from other wind profilers and from rawinsonde measurements (Strauch et al. 1987; Weber and Wuertz 1990; May 1993). Further studies comparing wind profiler observations with model analyses have also been conducted. Pauley et al. (1994) compared wind profiler observations with operational regional analyses at a site in Illinois. Schafer et al. (2003) studied the differences between wind profiler measurements and model winds (from the NCEP–NCAR reanalysis) at locations in the tropical Pacific, which is a region with few observations. Both studies showed that assimilation of wind profiler observations resulted in an improvement to the model analyses.

Wind profilers are designed to detect the motion of the air due to refractive index irregularities (Bragg scattering; Bailey 2000). Data can, however, be contaminated by competing motion from objects in the air such as birds and, more important, hydrometeors (Rayleigh scattering). The wind data utilized here were measured in 2012 by a network of wind profilers around the United Kingdom: Aberystwyth (52.424°N , 4.005°W); Camborne (50.219°N , 5.327°W); Douglas, Isle of Man (54.107°N , 4.553°W); Dunkeswell (50.860°N , 3.240°W); South Uist (57.254°N , 7.375°W); and Wattisham (52.124°N , 0.956°E). Data at each location are available at fixed heights above mean sea level. The data from Aberystwyth and South Uist have an averaging time of 30 min, while the data for the other sites are available as both 15- and 30-min averages. There are some differences among the instrumentation at the various sites.

The wind profilers at Camborne, Douglas, Dunkeswell, and Wattisham are all Vaisala LAP3000 wind profilers

with an antenna array about 5 m across. These operate at either 1290 or 915 MHz and routinely measure up to heights of around 3 km. They are capable of measuring up to around 3 km in “normal” clear-sky conditions, as long as the atmosphere is sufficiently moist. If the atmosphere is dry, the returned power is lower and this can result in layers of missing data or a reduction in the maximum measurable altitude. Because of their operating frequency, they are significantly affected by scattering from hydrometeors, but otherwise measure scattering from the air. Thick clouds produce strong scattering at the wind profiler’s operating frequency, and, as a result, under these conditions the wind profilers are capable of producing data up to approximately 8 km.

The wind profiler at South Uist is a 64-MHz LAP12000 system, designed to be able to measure up to around 12 km, although it rarely reached that height in 2012 because of a gradual decline in performance because of age and difficulties in “tuning” the phase of the system’s transmitters during scheduled maintenance. The profiler has a powerful antenna array comprising a field of 144 antennas, each 2 m high, and the array is about 40 m across. The operating frequency is too low for the wind profiler to be affected by rainfall unless it is very heavy, so it generally only yields returns from the air. The profiler is affected by areas of dry air and certain types of flow that result in low returns, so gaps are sometimes seen in the data.

The wind profiler array at Aberystwyth is larger still with 400 antennas, each about 4 m tall, with a total array width of 110 m. This gives a maximum measurable altitude of around 20 km, although it is typically only used up to 16 km. It operates at 46.5 MHz, so it is even less likely to be affected by rainfall than the wind profiler at South Uist. When it is, however, it tends to mask the clear-air returns (resulting in gaps in the data) rather than contaminating them with scattering from the precipitation. It is a much more powerful array—the most powerful in the United Kingdom—so it rarely suffers from gaps in the data.

b. Free-troposphere results

The Aberystwyth and South Uist wind profilers consistently report data above the boundary layer, and data from these two wind profilers are available at 30-min intervals. Figure 3 compares spectra at selected example heights at Aberystwyth and South Uist, calculated from wind profiler observations during 2012 and from MetUM NWP data.

The spectra from wind profiler observations and from NWP data were calculated with the same method as used for the boundary layer data, except that the point of divergence was not limited by the diurnal cycle (in fact

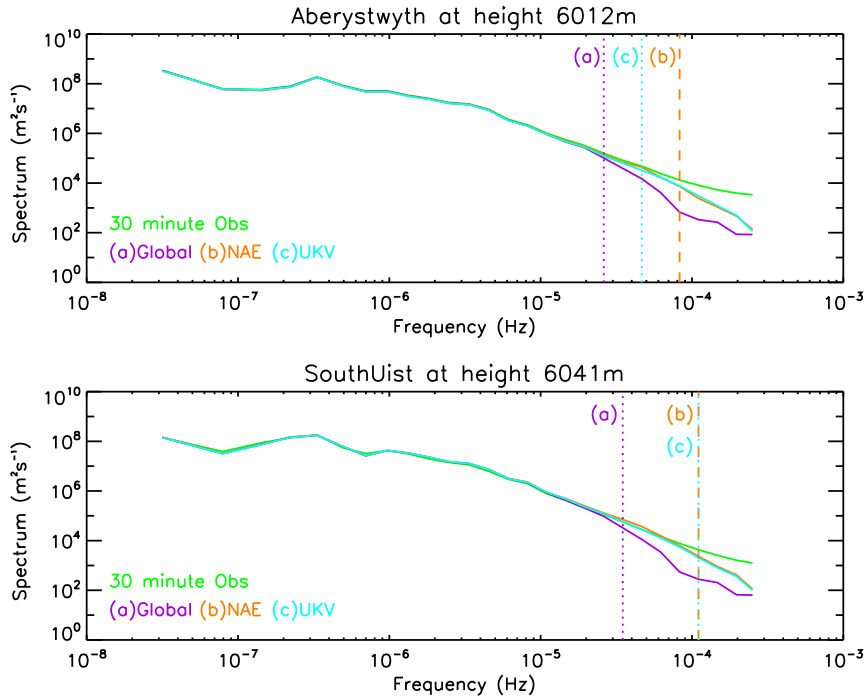


FIG. 3. Example free-tropospheric spectra at Aberystwyth and South Uist generated from wind profiler observations (30-min mean) and MetUM data [global (25 km, 3 h), NAE (12 km, 1 h), and UKV (1.5 km, 1 h)]. The dashed and dotted vertical lines [labeled (a)–(c)] indicate the frequency at which the NWP spectra diverge from the observational spectra.

this would have made no difference) and no scaling factor was applied to the NWP spectra to ensure a match at low frequencies. The scaling factor should not be necessary as there are no local site effects, and in fact the spectra agree remarkably well at low frequencies. We note that there is more energy in motions of all frequencies in the free troposphere when compared with boundary layer motions (note the difference in the vertical axis values between Fig. 1 and Fig. 3), which is consistent with higher wind speeds in the free troposphere. In addition, Fig. 3 shows that the NWP spectra begin to diverge from the observations spectra at a higher frequency in the free troposphere. We see also that the spectra from hourly sampled NAE (12-km resolution) and UKV (1.5-km resolution) data are very similar, but both differ significantly from the spectrum obtained from 3-h sampled global (25-km resolution) data, which diverges from the observed spectra at a lower frequency and has noticeably more missing energy. This suggests that the time frequency of the NWP data is the limiting factor here in representing the higher-frequency motions in the free troposphere. Based on this, the NWP spectra obtained using hourly sampled 4km data are expected to be very similar to the spectra from hourly NAE and UKV data.

The missing variance in the NWP free-tropospheric spectra is calculated using the same method employed with the boundary layer spectra. A summary of the ranges of the velocity variance obtained across the different sites, a selection of heights above the boundary layer up to about 6km and different averaging times is given in Table 4. As expected, and as seen within the boundary layer, larger velocity variances for the unresolved motions are obtained from the global spectra than from the higher-resolution NAE and UKV models. The missing energy in the NAE and UKV models is, as expected, similar. In general, for a particular NWP model, the missing energy is similar at various free-tropospheric heights at any one wind profiler location (not shown) but there is significant variation in the missing energy between different locations (e.g., between Aberystwyth and South Uist). The data from South Uist have more missing observations than the data from Aberystwyth, but investigations, in which extra missing observations were artificially added to the Aberystwyth dataset, showed that this fact cannot explain the lower missing energy values. These differences between results from different wind profiler sites are not really understood, but it is possible that they may be due to different instrumentation or that results may be affected by calibration errors or model biases.

TABLE 4. The ranges of velocity variances ($\text{m}^2 \text{s}^{-2}$) and diffusivities ($\text{m}^2 \text{s}^{-1}$) obtained using wind profiler observations.

Model	Resolution	σ_u^2 ($\text{m}^2 \text{s}^{-2}$)	K_u ($\beta = 3$) ($\text{m}^2 \text{s}^{-1}$)	K_u ($\beta = 9$) ($\text{m}^2 \text{s}^{-1}$)
MetUM global	25 km, 3 h	0.77–2.79	5248–22 102	15 744–66 306
MetUM NAE	12 km, 1 h	0.16–0.92	407–2963	1221–8889
MetUM UKV	1.5 km, 1 h	0.11–1.17	243–4614	729–13 842

Figure 4 shows the correlation functions (normalized by the variance) for the motions corresponding to the missing energy in the free-tropospheric NWP spectra shown in Fig. 3. As before, the time taken for the normalized correlation function to fall to $1/e$ gives an Eulerian time scale that is used to determine an appropriate Lagrangian time scale. The largest time scales are obtained for the 3-hourly global NWP data. The similarities between the missing variance in the NAE and UKV data (both hourly) are also seen in the correlation functions, with similar time scales obtained.

Horizontal diffusivities are obtained from the velocity variances (calculated from the missing variance in the energy spectra) and the Lagrangian time scales (calculated from the correlation functions) using $K_u = \sigma_u^2 \tau_L$. Within the boundary layer, a Lagrangian time scale τ_L was obtained from the Eulerian time scale τ_E using $\tau_L = \beta \tau_E$ and assuming $\beta = 3$. The time scales τ_L and τ_E are

expected to satisfy $\tau_L/\tau_E \propto u/\sigma_u$, and an analysis of the observations used in this study, both at heights in the boundary layer and in the free troposphere, indicates that u/σ_u can be larger in the free troposphere by approximately a factor of 3 (not shown). Assuming $\tau_L = \beta \tau_E$, Table 4 gives the range of diffusivities, obtained over the different wind profiler locations, observing heights and averaging times studied, for two values of β : 3 (as chosen for the boundary layer) and 9 (based on the expected larger values of u/σ_u in the free troposphere). As was the case for the study of missing motions in the NWP data in the boundary layer, a wide range of diffusivities is obtained that is, in this case, due primarily to the differences seen between different wind profiler locations. The diffusivity values recommended for use within the boundary layer (see Table 3) lie within the $\beta = 3$ free-tropospheric ranges given in Table 4, except in the case of the NAE model. In the free troposphere,

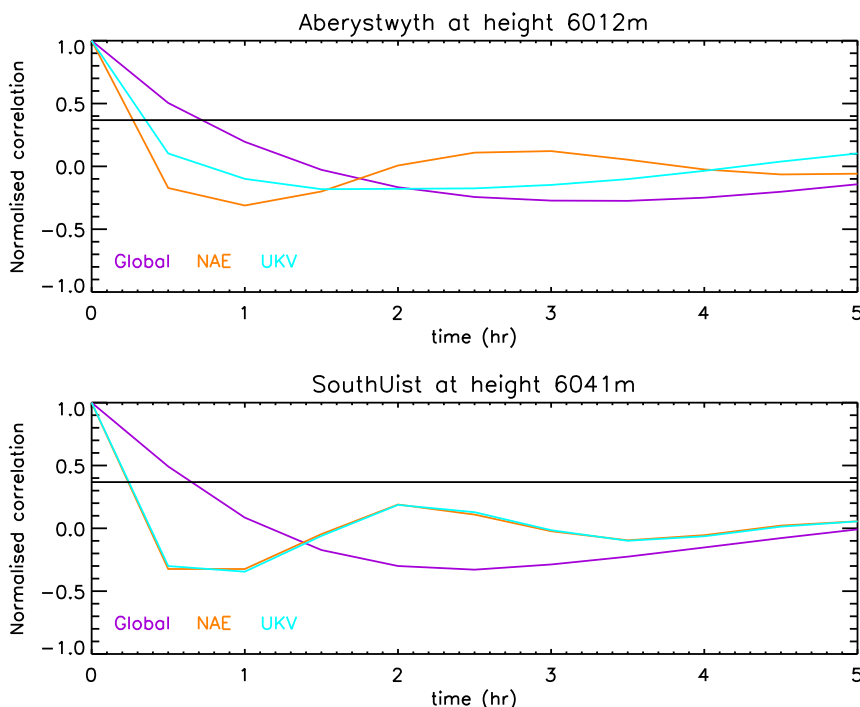


FIG. 4. Example normalized correlation functions for the unresolved mesoscale motions at selected heights at Aberystwyth and South Uist, generated from wind profiler observations (30 min) and MetUM data [global (25 km, 3 h), NAE (12 km, 1 h), and UKV (1.5 km, 1 h)]. The horizontal $1/e$ line (black) is used to determine the time scale.

the diffusivity due to the missing motions in the NAE model is much more similar to that in the UKV model than is the case for a similar comparison made within the boundary layer. This would be expected given the similarities seen between the NAE and UKV in the free-tropospheric energy spectra and correlation functions. The range of NAE diffusivity values obtained from data within the boundary layer do, however, overlap to some degree with the $\beta = 3$ range of NAE diffusivity values obtained from data within the free troposphere (see Tables 2 and 4) and agree quite well with the $\beta = 9$ NAE diffusivity values. The UKV free-tropospheric diffusivity values for $\beta = 9$ are somewhat larger than the corresponding boundary layer values, although with a wide range that is not inconsistent with the boundary layer range. For the global model with ~ 25 -km resolution, the free-troposphere results for $\beta = 9$ are significantly larger than the boundary layer results. Given the significant uncertainty in the free-tropospheric diffusivities, and the simplicity of adopting the same approach throughout, it is proposed that the recommended boundary layer diffusivities (see Table 3) be applied throughout the atmosphere. However, there could be a case for larger values above the boundary layer for models with coarser resolution.

6. Conclusions

Spectral analysis has been used to compare NWP and observed winds. This analysis has enabled the velocity variance, time scale, and implied diffusivity of the atmospheric motions that are missing in the NWP data to be estimated. Despite some uncertainty resulting from variations between results at different observing sites and from different time periods, there is strong evidence to suggest that the parameterization of unresolved mesoscale motions in atmospheric dispersion models should depend on the resolution of the input NWP data, with smaller parameterized variances and diffusivities required with data from higher-resolution NWP models.

In the boundary layer the results show that both the spatial resolution of the NWP model and the time interval at which data are extracted are important. However, for 3-h data, spatial resolution has little effect for grid spacing below ~ 20 km (see Tables 2 and 3) and, for hourly data, spatial resolution has little effect below ~ 4 km. This suggests that for these cases the time sampling is the dominant factor limiting the fidelity of the data. While the scatter is such that very definite conclusions are not possible, this is consistent with the idea that, for optimal results, the time resolution of the data should be proportional to the spatial resolution, reflecting the need to represent the time evolution

caused by advection of spatial structures by the large-scale wind.

In the free troposphere there is a large variation between results from different wind profiler sites that is not understood. This leads to significant uncertainty in the determined time scales and variances of the missing motions in the NWP data. For hourly NWP data within the free troposphere, spatial resolution has little clear effect below a resolution of ~ 12 km (and we do not have hourly NWP data available to test coarser resolutions). In comparison with the boundary layer results, this probably reflects the higher wind speeds in the free troposphere. Overall, the missing motions in the free troposphere have more variance, consistent with higher wind speeds aloft. The resulting diffusivities are, however, not too dissimilar to those obtained in the boundary layer, with the possible exception of the results from the coarsest NWP model that we considered in the free troposphere (with resolution ~ 25 km and 3-h data).

Taking account of the uncertainties involved and the benefits of a simple scheme that is spatially homogeneous, a parameterization of unresolved mesoscale motions is proposed, giving estimates for the velocity variance, Lagrangian time scale, and diffusivity based on the temporal and spatial resolution of the input NWP data. The values proposed are recommended for use in parameterizing unresolved mesoscale motions in atmospheric dispersion models driven by NWP wind fields. The results presented in this study are based on data within the United Kingdom but for a range of conditions, locations, altitudes, different terrains, instrumentation, and periods of time. In addition, NWP data from different models and centers are included. As such, results are expected to be applicable to NWP data of similar resolutions from other centers and at other geographical locations outside the United Kingdom. Nonetheless, to test this, further analysis at locations in other regions with different terrain features and climate would be beneficial.

As both the analysis in the boundary layer and the free troposphere showed, the key limiting factor in representing the higher-frequency atmospheric motions is the time sampling of the NWP data. Despite significant advances in NWP, with modeling being conducted at increasingly higher spatial resolution, the time sampling of the NWP data used for atmospheric dispersion models has not kept pace. This work suggests that to gain the full benefit of increases in spatial resolution of NWP modeling, more frequent time sampling is required. There would, therefore, be interest in repeating the analysis conducted here with higher-time-resolution NWP data. Increases in the temporal

resolution of input NWP data bring similar challenges to those encountered with spatial resolution increases, notably data storage, data transfer, and atmospheric dispersion model runtime.

Our focus in this paper has been to estimate, direct from wind velocities from NWP data and observations, the velocity variances and Lagrangian time scales for use in a parameterization of unresolved mesoscale motions. An alternative approach is to investigate the parameter values that lead to the best agreement between dispersion model predictions and tracer dispersion experiments. This is beyond the scope of this paper but is being considered in a separate study (V. Selvaratnam et al. 2018, unpublished manuscript in progress) using measurements from the Cross-Appalachian Tracer Experiment (CAPTEX) and the Across North America Tracer Experiment (ANATEX).

Acknowledgments. Use of observational data from the following sources is acknowledged: Met Office surface site observations, MRU Cardington surface site observations, and Met Office wind profiler data. The authors express their gratitude to the relevant teams and individuals within the Met Office for data provision, advice, and assistance.

REFERENCES

- Anfossi, D., D. Oettl, G. Degrazia, and A. Goulart, 2005: An analysis of sonic anemometer observations in low wind speed conditions. *Bound.-Layer Meteor.*, **114**, 179–203, <https://doi.org/10.1007/s10546-004-1984-4>.
- Bailey, D. T., 2000: Meteorological monitoring guidance for regulatory modeling applications. EPA Tech. Rep. EPA-454/R-99-005, 171 pp., <http://www.epa.gov/scram001/guidance/met/mmgrma.pdf>.
- Carruthers, D. J., R. J. Holroyd, J. C. R. Hunt, W. S. Weng, A. G. Robins, D. D. Apsley, D. J. Thomson, and F. B. Smith, 1994: UK-ADMS: A new approach to modelling dispersion in the earth's atmospheric boundary layer. *J. Wind Eng. Ind. Aerodyn.*, **52**, 139–153, [https://doi.org/10.1016/0167-6105\(94\)90044-2](https://doi.org/10.1016/0167-6105(94)90044-2).
- Clarke, R. H., 1979: A model for short and medium range dispersion of radionuclides released to the atmosphere. National Radiological Protection Board Rep. NRPB-R91, 79 pp.
- Davies, B. M., and D. J. Thomson, 1999: Comparisons of some parametrizations of wind direction variability with observations. *Atmos. Environ.*, **33**, 4909–4917, [https://doi.org/10.1016/S1352-2310\(99\)00287-3](https://doi.org/10.1016/S1352-2310(99)00287-3).
- Gupta, S., R. T. McNider, M. Trainer, R. J. Zamora, K. Knupp, and M. P. Singh, 1997: Nocturnal wind structure and plume growth rates due to inertial oscillations. *J. Appl. Meteor.*, **36**, 1050–1063, [https://doi.org/10.1175/1520-0450\(1997\)036<1050:NWSAPG>2.0.CO;2](https://doi.org/10.1175/1520-0450(1997)036<1050:NWSAPG>2.0.CO;2).
- Hanna, S. R., 1981a: Diurnal variation of horizontal wind direction fluctuations in complex terrain at Geysers, Cal. *Bound.-Layer Meteor.*, **21**, 207–213, <https://doi.org/10.1007/BF02033938>.
- , 1981b: Lagrangian and Eulerian time-scale relations in the daytime boundary layer. *J. Appl. Meteor.*, **20**, 242–249, [https://doi.org/10.1175/1520-0450\(1981\)020<0242:LAETSR>2.0.CO;2](https://doi.org/10.1175/1520-0450(1981)020<0242:LAETSR>2.0.CO;2).
- , 1983: Lateral turbulence intensity and plume meandering during stable conditions. *J. Climate Appl. Meteor.*, **22**, 1424–1430, [https://doi.org/10.1175/1520-0450\(1983\)022<1424:LTIAPM>2.0.CO;2](https://doi.org/10.1175/1520-0450(1983)022<1424:LTIAPM>2.0.CO;2).
- , 1990: Lateral dispersion in light-wind stable conditions. *Nuovo Cimento*, **13C**, 889–894, <https://doi.org/10.1007/BF02514777>.
- Jones, A. R., D. J. Thomson, M. Hort, and B. Devenish, 2007: The U.K. Met Office's next-generation atmospheric dispersion model, NAME III. *Air Pollution Modeling and Its Application XVII*, C. Borrego and A.-L. Norman, Eds., Springer, 580–589.
- Kristensen, L., N. O. Jensen, and E. L. Peterson, 1981: Lateral dispersion of pollutants in a very stable atmosphere—The effect of meandering. *Atmos. Environ.*, **15**, 837–844, [https://doi.org/10.1016/0004-6981\(81\)90288-2](https://doi.org/10.1016/0004-6981(81)90288-2).
- Luhar, A. K., 2012: Lagrangian particle modeling of dispersion in light winds. *Lagrangian Modeling of the Atmosphere, Geophys. Monogr.*, Vol. 200, Amer. Geophys. Union, 37–51.
- Maryon, R. H., 1997: Determining cross-wind variance for low-frequency wind meander. Met Office Turbulence and Diffusion Note 236, 32 pp.
- , 1998: Determining cross-wind variance for low frequency wind meander. *Atmos. Environ.*, **32**, 115–121, [https://doi.org/10.1016/S1352-2310\(97\)00325-7](https://doi.org/10.1016/S1352-2310(97)00325-7).
- May, P. T., 1993: Comparison of wind-profiler and radiosonde measurements in the tropics. *J. Atmos. Oceanic Technol.*, **10**, 122–127, [https://doi.org/10.1175/1520-0426\(1993\)010<0122:COWPAR>2.0.CO;2](https://doi.org/10.1175/1520-0426(1993)010<0122:COWPAR>2.0.CO;2).
- Moore, D. J., 1975: Observed and calculated magnitudes and distances of maximum ground level concentration of gaseous effluent material downwind of a tall stack. *Advances in Geophysics*, Vol. 18B, Academic Press, 201–221, [https://doi.org/10.1016/S0065-2687\(08\)60581-6](https://doi.org/10.1016/S0065-2687(08)60581-6).
- , 1976: Calculation of ground level concentration for different sampling periods and source locations. *Atmospheric Pollution: Proceedings of the 12th International Colloquium, Paris, France, May 5–7, 1976*, M. M. Benarie, Ed., Elsevier, 51–60.
- Mylne, K. R., 1992: Concentration fluctuation measurements in a plume dispersing in a stable surface layer. *Bound.-Layer Meteor.*, **60**, 15–48, <https://doi.org/10.1007/BF00122060>.
- , and P. J. Mason, 1991: Concentration fluctuation measurements in a dispersing plume at a range of up to 1000 m. *Quart. J. Roy. Meteor. Soc.*, **117A**, 177–206, <https://doi.org/10.1002/qj.49711749709>.
- Oettl, D., R. A. Almbauer, and P. J. Sturm, 2001: A new method to estimate diffusion in stable, low-wind conditions. *J. Appl. Meteor.*, **40**, 259–269, [https://doi.org/10.1175/1520-0450\(2001\)040<0259:ANMTED>2.0.CO;2](https://doi.org/10.1175/1520-0450(2001)040<0259:ANMTED>2.0.CO;2).
- Pasquill, F., and F. B. Smith, 1983: *Atmospheric Diffusion: A Study of the Dispersion of Windborne Material from Industrial and Other Sources*. 3rd ed. Ellis Horwood Limited, 437 pp.
- Pauley, P. M., R. L. Creasey, W. L. Clark, and G. D. Nastrom, 1994: Comparisons of horizontal winds measured by opposing beams with the Flatland ST radar and between Flatland measurements and NMC analyses. *J. Atmos. Oceanic Technol.*, **11**, 256–274, [https://doi.org/10.1175/1520-0426\(1994\)011<0256:COHWMB>2.0.CO;2](https://doi.org/10.1175/1520-0426(1994)011<0256:COHWMB>2.0.CO;2).
- Schacher, G. E., C. W. Fairall, and P. Zannetti, 1982: Comparison of stability classification methods for parameterizing coastal overwater dispersion. *Proc. First Int. Conf. on the Meteorology*

- and Air–Sea Interaction of the Coastal Zone, The Hague, Netherlands, Amer. Meteor. Soc., 91–96.
- Schafer, R., S. K. Avery, and K. S. Gage, 2003: A comparison of VHF wind profiler observations and the NCEP–NCAR reanalysis over the tropical Pacific. *J. Appl. Meteor.*, **42**, 873–889, [https://doi.org/10.1175/1520-0450\(2003\)042<0873:ACOVWP>2.0.CO;2](https://doi.org/10.1175/1520-0450(2003)042<0873:ACOVWP>2.0.CO;2).
- Smith, F. B., and P. F. Abbott, 1961: Statistics of lateral gustiness at 16 m above ground. *Quart. J. Roy. Meteor. Soc.*, **87**, 549–561, <https://doi.org/10.1002/qj.49708737409>.
- Stohl, A., 2000: The effect of unresolved mesoscale wind velocity fluctuations on dispersion model results. *Air Pollution and its Application XIII*, S. E. Gryning and E. Batchvarova, Eds., Springer, 311–320.
- , C. Forster, A. Frank, P. Seibert, and G. Wotawa, 2005: Technical note: The Lagrangian particle dispersion model FLEXPART version 6.2. *Atmos. Chem. Phys.*, **5**, 2461–2474, <https://doi.org/10.5194/acp-5-2461-2005>.
- Strauch, R. G., B. L. Weber, A. S. Frisch, C. G. Little, D. A. Merritt, K. P. Moran, and D. C. Welsh, 1987: The precision and relative accuracy of profiler wind measurements. *J. Atmos. Oceanic Technol.*, **4**, 563–571, [https://doi.org/10.1175/1520-0426\(1987\)004<0563:TPARAO>2.0.CO;2](https://doi.org/10.1175/1520-0426(1987)004<0563:TPARAO>2.0.CO;2).
- Weber, B. L., and D. B. Wuertz, 1990: Comparison of rawinsonde and wind profiler radar measurements. *J. Atmos. Oceanic Technol.*, **7**, 157–174, [https://doi.org/10.1175/1520-0426\(1990\)007<0157:CORAWP>2.0.CO;2](https://doi.org/10.1175/1520-0426(1990)007<0157:CORAWP>2.0.CO;2).
- Webster, H. N., and D. J. Thomson, 2005: Parameterising low-frequency meander in atmospheric dispersion models. *10th Int. Conf. on Harmonisation within Atmospheric Dispersion Modelling for Regulatory Purposes*, Crete, Greece, HARMO, 594–598, http://www.harmo.org/Conferences/Proceedings/_Crete/publishedSections/p594.pdf.
- , T. Whitehead, and D. J. Thomson, 2014: Parametrizing low-frequency mesoscale motions in atmospheric dispersion models. *16th Int. Conf. on Harmonisation within Atmospheric Dispersion Modelling for Regulatory Purposes*, Varna, Bulgaria, HARMO, H16-015, http://www.harmo.org/Conferences/Proceedings/_Varna/publishedSections/H16-015-Webster-EA.pdf.
- , —, and —, 2015: Parametrizing unresolved mesoscale motions in NAME. Forecasting Research Tech. Rep. 601, 134 pp., https://www.metoffice.gov.uk/binaries/content/assets/mohippo/pdf/q1/frtr_601_2015p.pdf.